Asia-Pacific Journal of Atmospheric Sciences (2018) 54:587–598
https://doi.org/10.1007/s13143-018-0080-5

Online ISSN 1976-7951
Print ISSN 1976-7633

ORIGINAL ARTICLE

Impacts of Aerosol Loading on Surface Precipitation from Deep Convective Systems over North Central Mongolia

Jambajamts Lkhamjav[1,2] · Hyunho Lee[1,3,4] · Ye-Lim Jeon[1] · Jaemyeong Mango Seo[1] · Jong-Jin Baik[1]

Received: 20 October 2017 / Revised: 31 January 2018 / Accepted: 14 March 2018 / Published online: 25 October 2018

Abstract

The impacts of aerosol loading on surface precipitation from mid-latitude deep convective systems are examined using a bin microphysics model. For this, a precipitation case over north central Mongolia, which is a high-altitude inland region, on 21 August 2014 is simulated with aerosol number concentrations of 150, 300, 600, 1200, 2400, and 4800 cm^{-3}. The surface precipitation amount slightly decreases with increasing aerosol number concentration in the range of 150–600 cm^{-3}, while it notably increases in the range of 600–4800 cm^{-3} (22% increase with eightfold aerosol loading). We attempt to explain why the surface precipitation amount increases with increasing aerosol number concentration in the range of 600–4800 cm^{-3}. A higher aerosol number concentration results in more drops of small sizes. More drops of small sizes grow through condensation while being transported upward and some of them freeze, thus increasing the mass content of ice crystals. The increased ice crystal mass content leads to an increase in the mass content of small-sized snow particles largely through deposition, and the increased mass content of small-sized snow particles leads to an increase in the mass content of large-sized snow particles largely through riming. In addition, more drops of small sizes increase the mass content of supercooled drops, which also leads to an increase in the mass content of large-sized snow particles through riming. The increased mass content of large-sized snow particles resulting from these pathways contributes to a larger surface precipitation amount through melting and collision-coalescence.

Keywords Aerosol loading impacts on surface precipitation · Deep convective systems · Bin microphysics scheme · WRF model · Mongolia

1 Introduction

Aerosols in the atmosphere play an important role in radiation processes and cloud and precipitation processes. They can serve as cloud condensation nuclei or ice nuclei. The sizes and chemical compositions of aerosols greatly influence the size distribution of nucleated drops in a cloud which subsequently affects the evolution of the cloud (Houze 2014). Aerosol-cloud-precipitation interactions have been recognized as an important issue in weather and climate research.

The impacts of aerosols on clouds and precipitation have been extensively investigated using numerical models, particularly focusing on how surface precipitation varies with aerosol number concentration (see review papers of Khain 2009; Tao et al. 2012; Fan et al. 2016). Many studies have shown that surface precipitation from shallow warm clouds decreases with increasing aerosol number concentration (Kuba and Fujiyoshi 2006; Xue and Feingold 2006; Cheng et al. 2007; Fan et al. 2012; Choi et al. 2014) while surface precipitation from deep convective clouds increases with increasing aerosol number concentration (Khain et al. 2005; Wang 2005; Rosenfeld et al. 2008; Igel et al. 2013; Clavner et al. 2017). The enhancement of surface precipitation from deep convective clouds with increasing aerosol number concentration has been explained by an invigoration of deep convective clouds when the environment is favorable for deep convection (e.g., high humidity). In a polluted environment, the mean radius of

Reponsible editor: Soon-Il An

✉ Jong-Jin Baik
jjbaik@snu.ac.kr

[1] School of Earth and Environmental Sciences, Seoul National University, Seoul 08826, Korea

[2] Department of Applied Mathematics, National University of Mongolia, Ulaanbaatar, Mongolia

[3] Center for Climate Systems Research, Columbia University, New York, NY, USA

[4] NASA Goddard Institute for Space Studies, New York, NY, USA

condensates is reduced (Twomey 1977) and the production of raindrops through collision-coalescence is inhibited. Instead, more cloud droplets are transported upward above the freezing level and then freeze while releasing latent heat, which consequently promotes updrafts and the formation of ice hydrometeors (Rosenfeld et al. 2008) and eventually enhances surface precipitation. The evaporation of raindrops in the boundary layer can strengthen the cold pool, which can facilitate the formation of secondary convection and thus enhance surface precipitation (Khain et al. 2005; Rosenfeld et al. 2008; O'Halloran et al. 2015).

On the other hand, some studies have shown that the relationship between surface precipitation amount and aerosol number concentration is not monotonic (Li et al. 2008; Ilotoviz et al. 2016; Alizadeh-Choobari and Gharaylou 2017; Dagan et al. 2017), implying that aerosol-cloud-precipitation interactions are rather complex. Li et al. (2008) demonstrated that the surface precipitation from deep convective clouds increases as the aerosol number concentration increases from clean marine to continental background conditions, but it is greatly decreased and completely suppressed under highly polluted conditions. Through real-case simulations, Alizadeh-Choobari and Gharaylou (2017) showed that the variation of surface precipitation amount with aerosol number concentration is non-monotonic, although the differences in surface precipitation amounts under the clean, control, and polluted conditions are not large (the control case showing the smallest amount of surface precipitation). They also showed that under the polluted condition light precipitation is reduced while both moderate and heavy precipitation are enhanced.

In the past two decades, numerical models with bin microphysics schemes have been broadly used to better understand clouds and precipitation and more accurately predict precipitation (e.g., Khain et al. 1999; Lynn et al. 2005; Khain et al. 2005; Tao et al. 2007; Khain 2009; Han et al. 2012; Iguchi et al. 2012; Xue et al. 2012; Lee et al. 2014; Khain et al. 2015; Xiao et al. 2015; Lee and Baik 2016; Tao and Li 2016; Gayatri et al. 2017; Sarangi et al. 2017). Numerical models with bin microphysics schemes predict the number concentration of each hydrometeor for each size bin. Accordingly, the size distributions of hydrometeors are better represented in numerical models with bin microphysics schemes than those with bulk microphysics schemes in which specified size-distribution functions are used. Hence, numerical models with bin microphysics schemes are more reliable in examining the impacts of aerosols on clouds and precipitation, although they require much more computational resources. However, real-case simulation studies of how gradual change of aerosol loading affects clouds and precipitation using numerical models with bin microphysics schemes have been rarely performed. This motivates the present study.

One of the components in bin microphysics schemes is the stochastic collection equation which describes the collisional growth of cloud particles. Recently, Lkhamjav et al. (2017a) evaluated an improved quasi-stochastic collection model which considers multiple collisions of cloud particles within a model time step. Through box model and idealized two-dimensional simulations, they showed that the onset of surface precipitation is accelerated compared to the normal quasi-stochastic collection model in which a cloud particle can experience only one collision with other cloud particle within a model time step. Using a numerical model that includes the improved quasi-stochastic collection model, Lkhamjav et al. (2017b) performed a prediction of precipitation over north central Mongolia and demonstrated that the improved quasi-stochastic collection model is indeed an improvement over the normal quasi-stochastic collection model. For the present study, we adopt a numerical model with the improved bin microphysics scheme (Lkhamjav et al. 2017a, b).

In this study, we investigate the impacts of aerosol loading on surface precipitation from mid-latitude deep convective systems through real-case simulations. A particular attempt is made to find pathways that lead to the variation of surface precipitation amount with aerosol loading. For the real case, a precipitation event that occurred over north central Mongolia is selected. The region is a high-altitude inland region and affected by natural and anthropogenic aerosols. An examination of aerosol loading impacts on surface precipitation in north central Mongolia can provide further insights into aerosol-cloud-precipitation interactions. This also motivates the present study. In section 2, the case description and experimental setup are briefly described. In section 3, the results and discussion are given. A summary and conclusions are provided in section 4.

2 Case Description and Experimental Setup

The case selected for this study is the 21 August 2014 precipitation event over north central Mongolia in Lkhamjav et al. (2017b). The 24-h accumulated surface precipitation amount that day was 30 mm in Ulaanbaatar and 19 mm in Darkhan. The two locations are indicated in Fig. 1a. In Mongolia, the average annual precipitation amount is ~210 mm, so the precipitation event with the 24-h accumulated surface precipitation amount of ~20–30 mm is unique. To see the synoptic environment of the precipitation event, the mean sea-level pressure and 850-hPa temperature field at 12 UTC 21 August 2014 is presented in Fig. 1a. This figure is adapted from Lkhamjav et al. (2017b). The low-level warm low is located southeast of Ulaanbaatar at 12 UTC 21 and moves northeastward. The low-level cold high is located northwest of Darkhan at 12 UTC 21 and moves southeastward. Near Darkhan, the gradients of pressure and temperature become

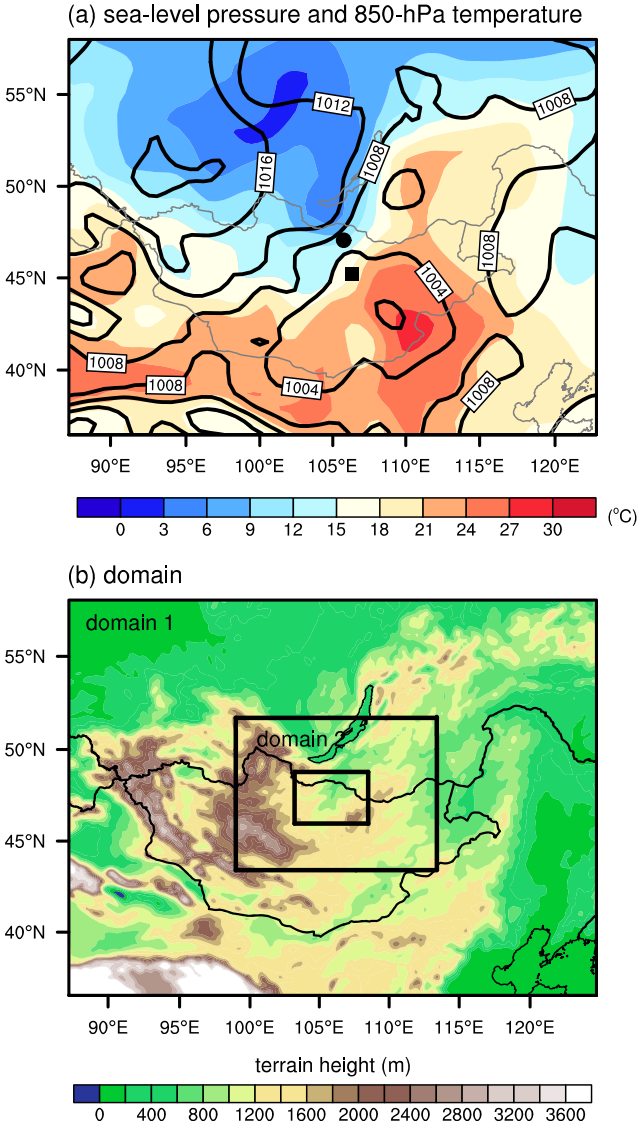

Fig. 1 **a** Field of mean sea-level pressure (hPa, black solid lines) and 850-hPa temperature (color shaded) at 12 UTC 21 August 2014 plotted using the ERA-Interim (0.75° × 0.75°) reanalysis data. The circle and square represent the locations of Darkhan and Ulaanbaatar observatories, respectively. **b** Two nested computational domains (domain 1 and domain 2) and terrain height. The innermost rectangular area represents the analysis area. [Adapted from Lkhamjav et al. 2017b]

large, implying the presence of a cold front. The precipitation event that occurred on 21 August 2014 is associated with the warm low and the cold front.

Figure 2 shows the time series of 2-m temperature, 2-m relative humidity, and 10-m wind speed and direction observed at Darkhan observatory. From ~10 UTC on 21 August, the temperature drops rapidly and the relative humidity increases abruptly for 1–2 h. For the 2-h period of 10–12 UTC, the decrease in 2-m temperature is 6.5 °C and the increase in 2-m relative humidity is 38%. The wind speed after ~10 UTC is stronger than that before ~10 UTC, and the wind direction after ~10 UTC changes very little (northwesterly). These features are evidence for the passage of the cold front at ~10 UTC at Darkhan.

The numerical model used in this study is the Weather Research and Forecasting (WRF) model coupled with the bin microphysics scheme of the Hebrew University Cloud Model (HUCM) (Lee and Baik 2016). In the bin microphysics scheme, seven hydrometeors [liquid drop, three types of ice crystals (column, plate, and dendrite), snow, graupel, and hail] and aerosol are considered and 43 mass-doubling bins are used to predict the number concentration of each hydrometeor in each bin and the aerosol number concentration in each bin. Microphysical processes included are activation, vapor diffusion, collision, secondary ice multiplication, breakup, freezing, and melting. The rimed fraction of snow is predicted. Also, the liquid water fractions of snow, graupel, and hail are predicted. The rimed fraction of snow is utilized for calculations of the density and terminal velocity of snow particles. As the rimed fraction of a snow particle is large, the snow particle resembles in characteristics a graupel particle or a hail particle. The type conversion from snow to graupel or hail is allowed according to the rimed fraction of snow. A time-dependent gradual melting process is included in the bin microphysics scheme. To calculate the time-dependent gradual melting, the liquid water fractions of snow, graupel, and hail are used. Deposition nucleation, condensation-freezing nucleation, immersion freezing, and secondary ice crystal formation are included to consider the formation of ice nuclei. For further details of the bin microphysics scheme, see Khain et al. (2000, 2011) and Lee and Baik (2016). The improved quasi-stochastic collection model is implemented in the bin microphysics scheme (Lkhamjav et al. 2017a, b). The turbulence-induced collision enhancement is not included in the present study.

The experimental setup is the same as that in Lkhamjav et al. (2017b). Figure 1b shows two one-way nested computational domains: the outer domain (domain 1) with a horizontal grid size of 15 km and the inner domain (domain 2 with a horizontal grid size of 5 km). The ERA-interim reanalysis data (Dee et al. 2011) are used to provide initial and boundary conditions for the WRF model. Table 1 shows the experimental setup.

Following Khain et al. (2000) and Lee et al. (2014), the initial size distribution of aerosol number concentration $N(r_a)$ is given by

$$\frac{dN}{d\ln r_a} = \frac{3}{2} N_0 k \left(\frac{4A^3}{27 B r_a^3} \right)^{k/2}. \quad (1)$$

Here, r_a is the aerosol radius, N_0 is the cloud condensation nucleus (CCN) number concentration at 1% supersaturation, k (= 0.5) is a constant, and A and B are coefficients related to the curvature and solution effects, respectively. The radius of

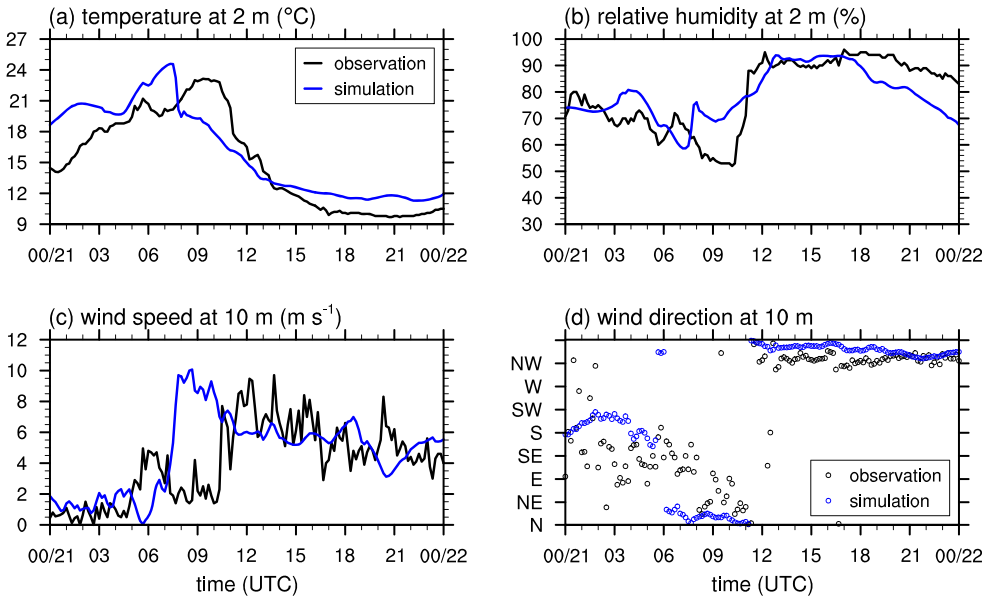

Fig. 2 Time series of (**a**) temperature at 2 m, (**b**) relative humidity at 2 m, (**c**) wind speed at 10 m, and (**d**) wind direction at 10 m from 00 UTC 21 to 00 UTC 22 August 2014 observed and simulated at Darkhan. The simulation case is the case of $N_0 = 600$ cm^{-3}

the largest aerosol is 2 μm. In nature, the ratio of the number of CCNs to the number of aerosols depends on the hygroscopicity of aerosols which differs according to aerosol types. In Eq. (1), N_0 and k reflect the hygroscopicity and thus determine the number concentration of aerosols that serve as CCNs. In this study, all aerosols are considered to be hygroscopic and the aerosol radius is regarded as the CCN radius. Note that the aerosols considered in this study are water-friendly aerosols. To examine the impacts of aerosol loading on surface precipitation amount, six numerical experiments are carried out with initial aerosol number concentrations of $N_0 = 150$, 300, 600, 1200, 2400, and 4800 cm^{-3}. The initial aerosol number concentration in the vertical is uniform up to 2 km height above the surface and then decreases exponentially with an e-folding height of 2 km. In Lkhamjav et al. (2017b), $N_0 = 300$ cm^{-3} was used. During the simulation period, aerosols are replenished using the scheme in Jiang and Wang (2014) in which the aerosol number concentration is adjusted toward the initial aerosol number concentration with a relaxation time. The aerosol number concentration at the lateral boundaries of domain 1 in each simulation is forced to follow the initial aerosol number concentration in the simulation.

The WRF model is integrated for 36 h starting from 12 UTC 20 August 2014. The first 12-h period is considered as the model spin-up period which is needed for the model to adjust to initial conditions. The last 24-h simulation data are used for the analysis. For further details of the case synopsis, numerical model, and experimental setup, see Lkhamjav et al. (2017b).

3 Results and Discussion

The model simulation is evaluated using observation data. For this, simulated 2-m temperature, 2-m relative humidity, and 10-m wind speed and direction in the case of $N_0 = 600$ cm^{-3} are compared to the observed ones (Fig. 2). In the simulation, the cold-front passes Darkhan 2–3 h earlier compared to the

Table 1 Experimental setup for this study

	Domain 1	Domain 2
Horizontal grid dimension	217 × 163	247 × 187
Horizontal grid size	15 km	5 km
Vertical grid number	42	42
Time step	60 s	20 s
Subgrid-scale cumulus	Kain-Fritsch (Kain 2004)	none
Microphysics	bin microphysics (Khain et al. 2000, 2011; Lee and Baik 2016)	
PBL	YSU (Hong et al. 2006)	
Land surface	Noah (Chen and Dudhia 2001)	
Longwave/Shortwave radiation	RRTMG (Iacono et al. 2008)	
Initial/Boundary conditions	ERA-Interim reanalysis (6-h intervals, 0.75° × 0.75° resolution)	

observation. Accordingly, the sudden decrease in temperature, the sudden increases in relative humidity and wind speed, and the shift of wind direction occur 2–3 h earlier in the simulation than in the observation. This earlier passage of the cold front makes a contribution to the differences in 2-m temperature, 2-m relative humidity, and 10-m wind speed and direction between the simulation and observation. The root-mean-square error is 2.7 °C for 2-m temperature, 9.2% for 2-m relative humidity, 2.8 m s^{-1} for 10-m wind speed, and 65° for 10-m wind direction. In spite of the earlier passage of the cold front, the time series of the simulated temperature, relative humidity, and wind speed and direction show the distinct features associated with the passage of the cold front.

To understand how and why the surface precipitation amount from the deep convective systems over north central Mongolia varies as the aerosol number concentration increases, we have analyzed surface precipitation amount, mass contents and number concentrations of hydrometeors, mass change rates of hydrometeors and water vapor due to microphysical processes, and size distributions of hydrometeors. Figure 3 shows the distributions of 24-h accumulated surface precipitation amount in the analysis area from 00 UTC 21 to 00 UTC 22 August 2014 for initial aerosol number concentrations of N_0 = 150, 300, 600, 1200, 2400, and 4800 cm^{-3}. The observed 24-h accumulated surface precipitation amount is given in Lkhamjav et al. (2017b). Overall, the spatial distributions of accumulated surface precipitation amount, which are associated with the warm low and the cold front, are similar. Major rainbands are elongated in the southwest-northeast direction. Despite the similarities, some differences in the fine

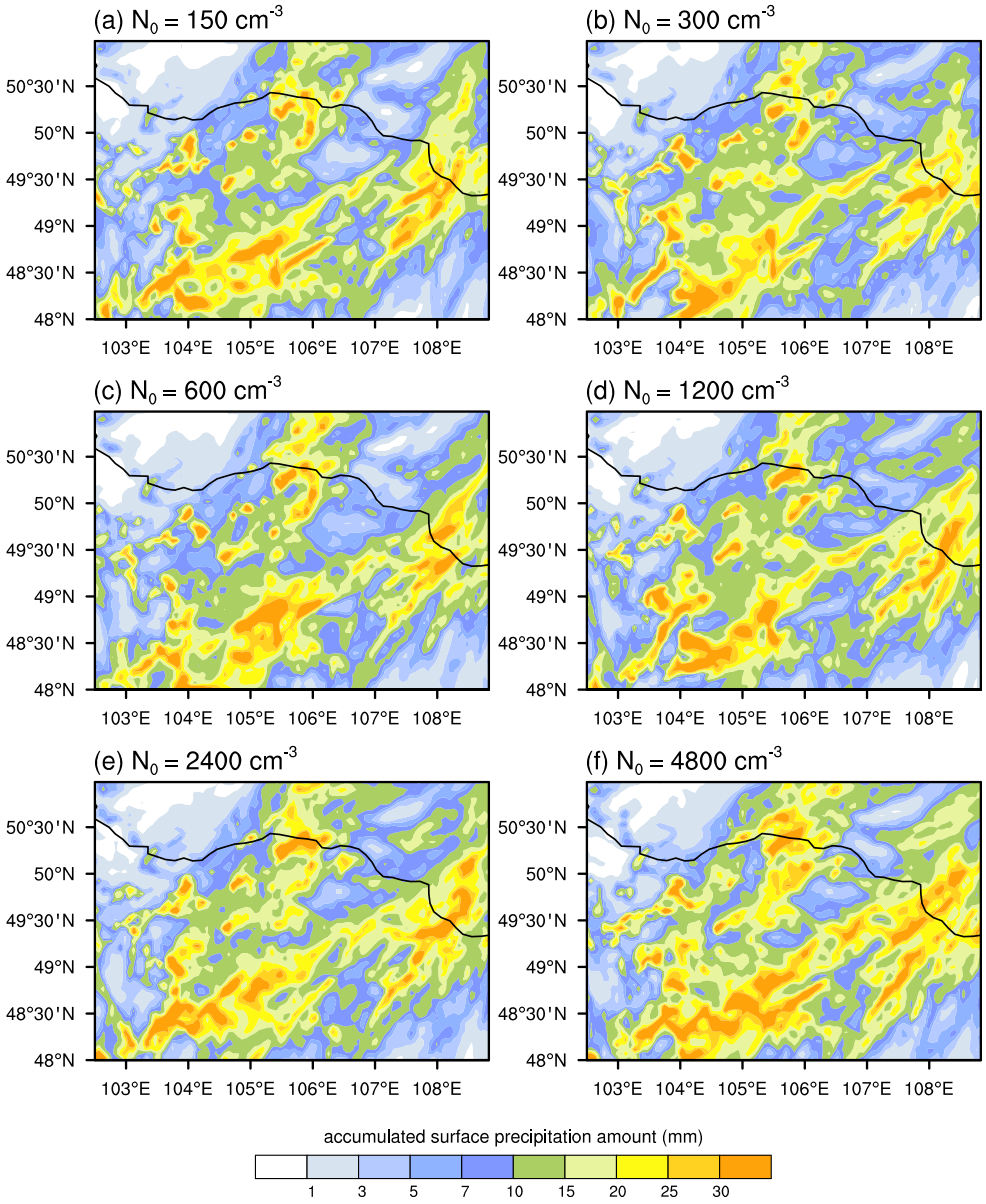

Fig. 3 Distributions of accumulated surface precipitation amount in the analysis area from 00 UTC 21 to 00 UTC 22 August 2014 in the cases of aerosol number concentrations of N_0 = (**a**) 150, (**b**) 300, (**c**) 600, (**d**) 1200, (**e**) 2400, and (**f**) 4800 cm^{-3}. The case of N_0 = 300 cm^{-3} is the same as in Lkhamjav et al. (2017b)

structure and amount of surface precipitation are also evident. For example, in the case of $N_0 = 4800$ cm^{-3}, the rainband elongated in the southwest-northeast direction in the southern region of the analysis area is longer and stronger than those in the other cases.

Figure 4 shows the averaged 24-h accumulated surface precipitation amount as a function of the initial aerosol number concentration. The average is taken over the analysis area. The non-monotonic behavior of the accumulated surface precipitation amount is seen as the aerosol number concentration changes. This kind of non-monotonic behavior has been reported in several other studies (Ilotoviz et al. 2016; Alizadeh-Choobari and Gharaylou 2017). In Alizadeh-Choobari and Gharaylou (2017), the accumulated surface precipitation amount is larger in the clean and polluted cases than in the control case. In the range of $N_0 = 150$–600 cm^{-3}, the accumulated surface precipitation amount slightly decreases with increasing aerosol number concentration. On the other hand, in the range of $N_0 = 600$–4800 cm^{-3}, there is a notable increase in accumulated surface precipitation amount with increasing aerosol number concentration. The increasing trend of surface precipitation with increasing aerosol number concentration has been reported in many studies (e.g., Wang 2005; Lee et al. 2008; Zhou et al. 2017). Several studies support the hypothesis that greater aerosol loading leads to an invigoration of deep convective systems (Khain et al. 2005; Lee et al. 2008; Rosenfeld et al. 2008). In the present study, the 24-h accumulated surface precipitation amount averaged over the analysis area in the case of $N_0 = 4800$ cm^{-3} (13.9 mm) is 22% larger than that in the case of $N_0 = 600$ cm^{-3} (11.4 mm). The analysis

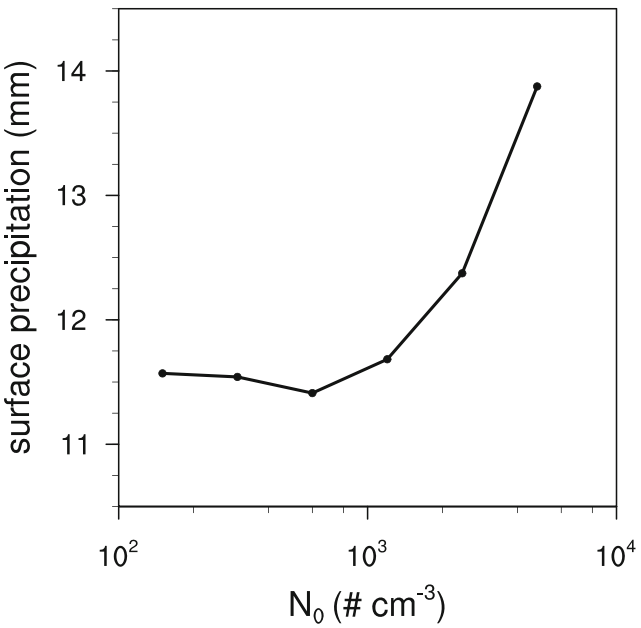

Fig. 4 Accumulated surface precipitation amount from 00 UTC 21 to 00 UTC 22 August averaged over the analysis area as a function of the initial aerosol number concentration

of the time series of surface precipitation rate averaged over the analysis area indicates that there is virtually no delay of surface precipitation caused by higher aerosol loading in the range of $N_0 = 600$–4800 cm^{-3} (not shown).

Li et al. (2008) investigated aerosol-cloud-precipitation interactions in deep convective clouds over Texas, USA using the WRF model that includes the two-moment bulk microphysics scheme. They showed that the accumulated surface precipitation amount slightly increases when the aerosol (CCN) number concentration goes from 100 to 1000 cm^{-3}, markedly and then slightly increases when the aerosol number concentration goes from 1000 to 4000–5000 cm^{-3}, and sharply decreases when the aerosol number concentration is above 5000 cm^{-3}. Interestingly, the precipitation is completely suppressed when the aerosol number concentration is 30000 cm^{-3}. The result showing the increase in accumulated surface precipitation amount with increasing aerosol number concentration in the range of $N_0 = 600$–4800 cm^{-3} (this study) is qualitatively consistent with the result in Li et al. (2008). Under very high aerosol conditions, it might be difficult for hydrometeors to grow into sufficiently large particles. Environmental conditions as well as changes in microphysical processes are responsible for that. Li et al. (2008) mentioned that under very high aerosol conditions the precipitation can be decreased or suppressed in relatively small wind shear and humid air. Therefore, it is possible that the surface precipitation amount would not continue to monotonically increase even as the aerosol number concentration increases. In this situation, there can be a certain aerosol number concentration beyond which the surface precipitation amount would decrease with increasing aerosol number concentration. This threshold value would depend on many factors such as environmental humidity, environmental wind shear, and the type of deep convection. It would be interesting to examine and find explanations for the variation of accumulated surface precipitation amount with increasing aerosol number concentration in the range of N_0 exceeding 4800 cm^{-3}, specifically for the precipitation event considered in this study. This deserves an investigation.

Next, we attempt to explain why the accumulated surface precipitation amount increases with increasing aerosol number concentration in the range of $N_0 = 600$–4800 cm^{-3}. The vertical profiles of hydrometeor mass contents in the case of $N_0 = 4800$ cm^{-3} and differences in hydrometeor contents between the case of $N_0 = 4800$ cm^{-3} and the case of $N_0 = 600$ cm^{-3} averaged over the 24-h period and the analysis area are presented in Fig. 5a and b, respectively. In Fig. 5 (also Figs. 6, 7, and 8), the axis label height stands for the vertical distance from the mean sea level. The average topographic height in the analysis area is ~1200 m. The freezing level is $z \sim 4$ km. Figure 5a shows that the snow mass content is the largest among the hydrometeor types, followed by the ice crystal mass content. The snow mass content is maximal at z

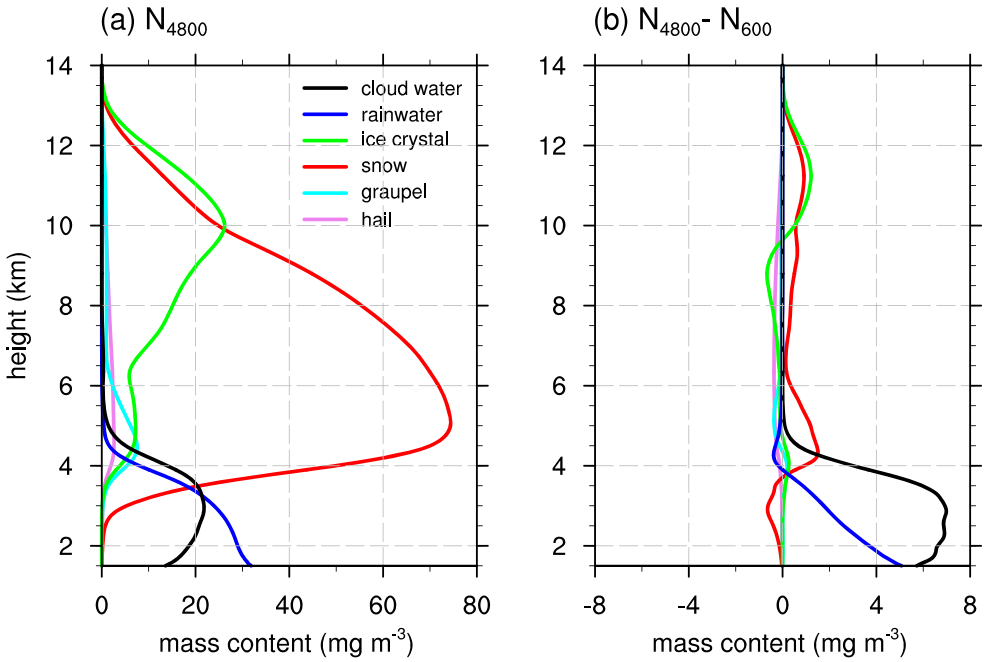

Fig. 5 **a** Vertical profiles of hydrometeor mass contents averaged over 24 h from 00 UTC 21 to 00 UTC 22 August 2014 and the analysis area in the case of $N_0 = 4800$ cm^{-3}. **b** Vertical profiles of differences in hydrometeor mass contents between the case of $N_0 = 4800$ cm^{-3} and the case of $N_0 = 600$ cm^{-3}

~ 5 km, and the ice crystal mass content is maximal at $z \sim 10$ km. Some snow particles are seen below the freezing level because of their gradual melting. Below $z \sim 3$ km, the rainwater mass content is the largest. The mass content of supercooled drops is largely concentrated between the freezing level and $z \sim 5$ km. Although the graupel mass content is much smaller than that of snow or ice crystal, it is notably concentrated between $z \sim 4$ km and $z \sim 6$ km. Hail is also seen, but the hail mass content is small.

Above the freezing level, the snow mass content is consistently larger in the case of $N_0 = 4800$ cm^{-3} than in the case of $N_0 = 600$ cm^{-3} (Fig. 5b). The cloud water and rainwater mass contents are notably larger in the case of $N_0 = 4800$ cm^{-3} than in the case of $N_0 = 600$ cm^{-3} (Fig. 5b). As will be presented later, the increased snow mass content is responsible for an increase in rainwater mass content. The increase in cloud water mass content is particularly pronounced between $z \sim 2$ km and $z \sim 3$ km. The increase in cloud water mass content above the freezing level means the increase in the amount of supercooled cloud droplets in the case of $N_0 = 4800$ cm^{-3}. The rainwater mass content also increases below the freezing level in the case of $N_0 = 4800$ cm^{-3}. This is attributed to an increase in the melting of snow particles and an increase in the collisional growth of raindrops produced by the melting of snow particles in the layer with a larger cloud water mass content.

Figure 6 shows the vertical profiles of the number concentrations of cloud drops (cloud droplets), ice crystals, and raindrops averaged over the 24-h period and the analysis area in the cases of $N_0 = 600$ and 4800 cm^{-3}. The cloud drop number concentration is consistently higher in the case of $N_0 = 4800$ cm^{-3} than in the case of $N_0 = 600$ cm^{-3} due to the higher aerosol number concentration. The maximum number concentration of cloud drops is ~4030 L^{-1} (per one liter of air) at $z \sim 3$ km in the case of 4800 cm^{-3} and ~2460 L^{-1} at $z \sim 3$ km in the case of 600 cm^{-3}, ~1.6 times larger in the case of $N_0 = 4800$ cm^{-3}. The ice crystal number concentration is also consistently higher in the case of $N_0 = 4800$ cm^{-3} than in the case of $N_0 = 600$ cm^{-3}. In both the cases, the maximum number concentration of ice particles is seen just above the freezing level. Just above the freezing level, some portion of the cloud drops transported below the freezing level freeze, forming ice crystals (Fig. 6a and b). The higher number concentration and smaller mass content of ice crystals mean that the average size of ice crystals is smaller in the case of $N_0 = 4800$ cm^{-3} than in the case of $N_0 = 600$ cm^{-3} (Figs. 5b and 6b). On the other hand, the raindrop number concentration is consistently lower in the case of $N_0 = 4800$ cm^{-3} than in the case of $N_0 = 600$ cm^{-3}. The lower number concentration and larger mass content of raindrops mean that the average size of raindrops is larger in the case of $N_0 = 4800$ cm^{-3} than in the case of $N_0 = 600$ cm^{-3} (Figs. 5b and 6c). In the case of $N_0 = 4800$ cm^{-3}, the average size of ice crystals is small, but the average size of raindrops is large. This implies that the growth of small-sized ice crystals through mixed-phased processes is important.

Figure 7a shows the vertical profiles of the mass change rates of hydrometeors and water vapor due to deposition, sublimation, condensation, evaporation, freezing, melting, riming, and nucleation averaged over the 24-h period and the analysis area in the case of $N_0 = 4800$ cm^{-3}. Here, the mass change rate due to a microphysical process means the rate of increase of the mass of water vapor, liquid water or ice produced through the microphysical process. For example, the mass change rate due to condensation means the rate of

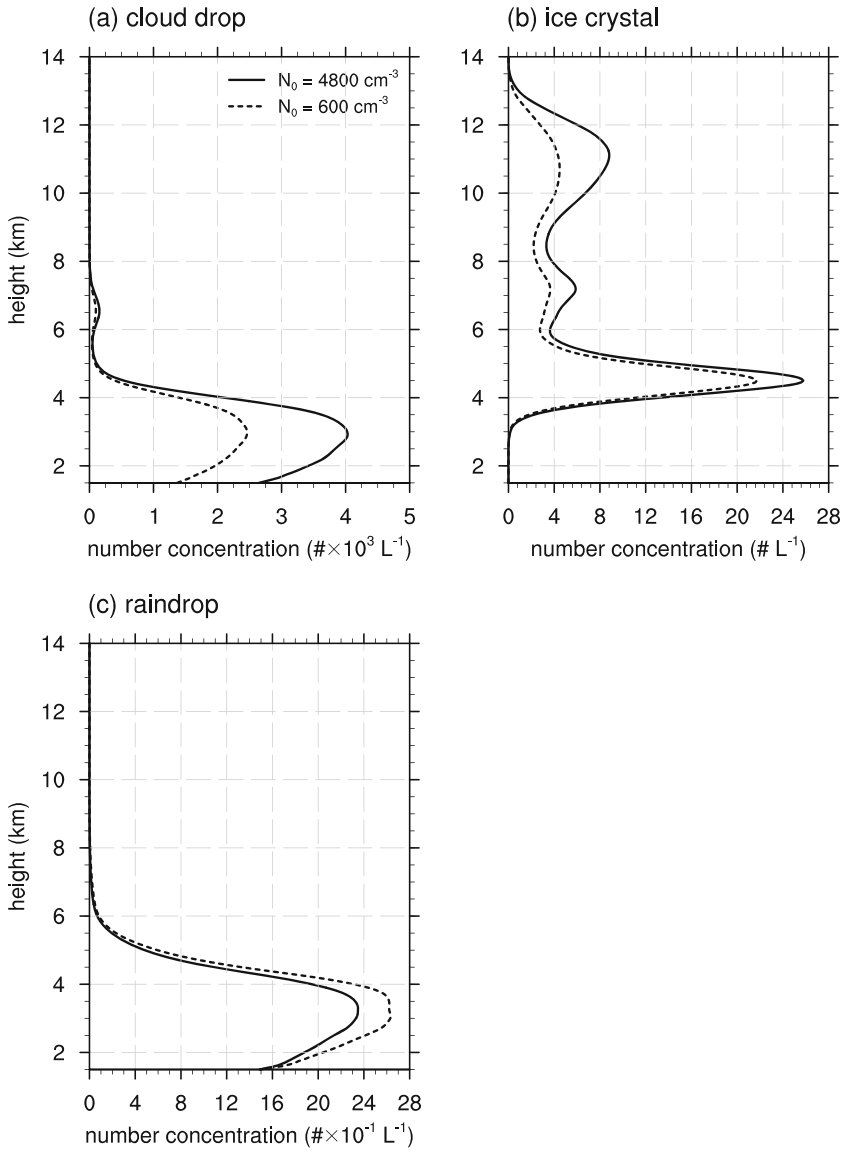

Fig. 6 Vertical profiles of the number concentrations of (**a**) cloud drops, (**b**) ice crystals, and (**c**) raindrops averaged over 24 h from 00 UTC 21 to 00 UTC 22 August 2014 and the analysis area in the cases of $N_0 = 600$ cm^{-3} and 4800 cm^{-3}

increase of the mass of liquid water due to condensation. Note that for ease of visualization the mass change rate due to nucleation is amplified 10 times in Fig. 7. Overall, the mass change rate due to deposition is much larger than that of sublimation and the mass change rate due to condensation is larger than that of evaporation. On the other hand, overall, the mass change rate due to freezing is smaller than that of melting. The mass change rate due to riming is notable, whose peak is located at $z \sim 4$ km and whose peak magnitude is comparable to that of the mass change rate due to deposition or condensation. The mass change rate due to nucleation is negligible. From Figs. 5a and 7a, we can deduce that the deposition in the mid- and upper troposphere is mainly responsible for the snow mass content and the growth of snow particles through riming is effective near the freezing level.

Differences in the mass change rates of hydrometeors and water vapor due to microphysical processes (Fig. 7b) reveal increases in riming, evaporation, and condensation in the case of $N_0 = 4800$ cm^{-3} relative to the case of $N_0 = 600$ cm^{-3}. The maximum increases in the mass change rates due to riming, evaporation, and condensation are seen at $z \sim 4$, 3, and 2 km, respectively. A higher aerosol number concentration produces more drops of small sizes. Thus, the totaled surface area of drops is larger and accordingly the diffusional growth of drops becomes stronger (Lee et al. 2014), which is reflected in the larger mass change rate due to condensation in the case of $N_0 = 4800$ cm^{-3} relative to the case of $N_0 = 600$ cm^{-3} (Fig. 7b). As discussed earlier, the average size of ice crystals is smaller, while the number concentration of ice crystals is higher in the case of $N_0 = 4800$ cm^{-3} than in the case of $N_0 = 600$ cm^{-3}. This is reflected in the fact that the mass change rate due to freezing is lower in the case of $N_0 = 4800$ cm^{-3} than in the case of $N_0 = 600$ cm^{-3} (Fig. 7b). The mass change rate due to melting is overall lower in the case of $N_0 = 4800$ cm^{-3} than

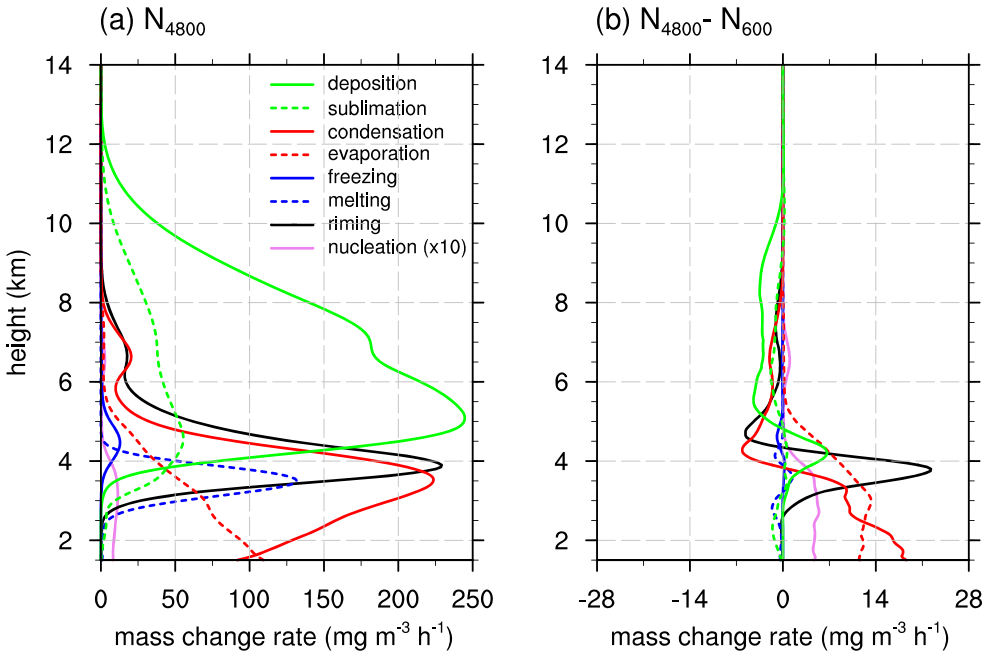

Fig. 7 **a** Vertical profiles of the mass change rates (see text) of hydrometeors and water vapor due to deposition, sublimation, condensation, evaporation, freezing, melting, riming, and nucleation (amplified 10 times) processes averaged over 24 h from 00 UTC 21 to 00 UTC 22 August 2014 and the analysis area in the case of $N_0 = 4800$ cm^{-3}. **b** Vertical profiles of differences in the mass change rates of hydrometeors and water vapor due to deposition, sublimation, condensation, evaporation, freezing, melting, riming, and nucleation (amplified 10 times) processes between the case of $N_0 = 4800$ cm^{-3} and the case of $N_0 = 600$ cm^{-3}

in the case of $N_0 = 600$ cm^{-3} except for the layer just below the freezing level. As will be shown below, however, the number concentration of snow particles is higher in the case of $N_0 = 4800$ cm^{-3} than in the case of $N_0 = 600$ cm^{-3}, contributing to an increase in the mass content of raindrops through melting and active collision-coalescence.

Figure 8 shows the mass size distributions of drops at $z = 3$ km and snow at $z = 5$ km and the number size distributions of

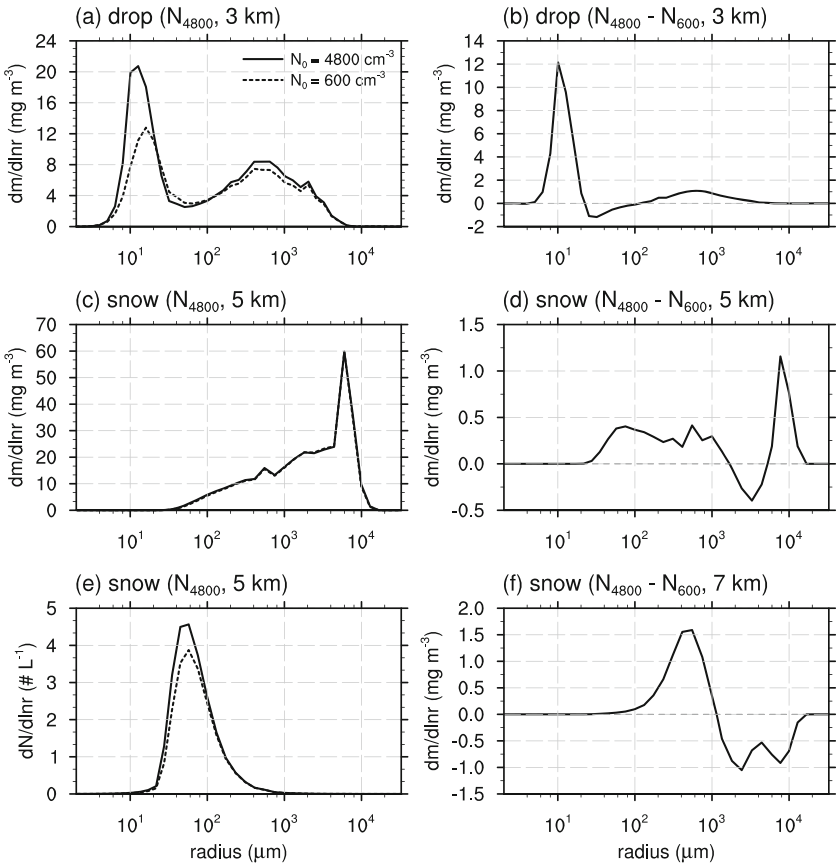

Fig. 8 Mass size distributions of (**a**) drops at $z = 3$ km and (**c**) snow at $z = 5$ km and number size distributions of (**e**) snow at $z = 5$ km in the cases of $N_0 = 4800$ cm^{-3} and 600 cm^{-3}. Differences in the mass size distributions of (**b**) drops at $z = 3$ km, (**d**) snow at $z = 5$ km, and (**f**) snow at $z = 7$ km between the case of $N_0 = 4800$ cm^{-3} and the case of $N_0 = 600$ cm^{-3}. All the size distributions are obtained by averaging over 24 h from 00 UTC 21 to 00 UTC 22 August 2014 and the analysis area

snow at $z = 5$ km averaged over the 24-h period and the analysis area in the cases of $N_0 = 600$ and 4800 cm^{-3}. The differences in the size distributions of drops at $z = 3$ km, snow at $z = 5$ km, and snow at $z = 7$ km between the case of $N_0 = 4800$ cm^{-3} and the case of $N_0 = 600$ cm^{-3} are also shown. At $z = 3$ km, the drop mass content in the radius range of ~6–15 μm, which belongs to a size range of cloud droplets, is particularly larger in the case of $N_0 = 4800$ cm^{-3} than in the case of $N_0 = 600$ cm^{-3} (Fig. 8a and b). This result means that more drops of small sizes form as the aerosol number concentration is higher. The maximum difference in the mass size distribution of drops is seen at the radius ~10 μm. More drops of small sizes increase the total surface area of drops, resulting in stronger low-level condensation (Fig. 7b). In addition, more drops of small sizes contribute to increases in ice crystals and supercooled drop mass contents above the freezing level (Fig. 5b).

The mass size distributions of snow at $z = 5$ km in the cases of $N_0 = 600$ and 4800 cm^{-3} are similar and exhibit a high peak at ~6 mm (Fig. 8c). In the case of $N_0 = 4800$ cm^{-3}, more cloud droplets result in more ice crystals through freezing (Figs. 5b and 8a). More ice crystals are grown into more small-sized snow particles near the freezing level largely through deposition (Figs. 5b, 7b, and 8e). As a result, the mass content of small-sized snow particles is larger in the case of $N_0 =$ 4800 cm^{-3} than in the case of $N_0 = 600$ cm^{-3} (Fig. 8d). In addition, the mass content of large-sized snow particles is larger in the case of $N_0 = 4800$ cm^{-3} than in the case of $N_0 =$ 600 cm^{-3} in the radius range of ~6–15 mm with a peak at ~8 mm (Fig. 8d). By comparing Fig. 8d and f, we can deduce that the increased mass content of large-sized snow particles is largely due to riming. More snow particles of large sizes which grow through riming melt to form relatively large drops. The relatively large drops collect drops of small sizes (collision-coalescence process), which leads to an enhanced surface precipitation amount.

Van den Heever et al. (2006) and Fan et al. (2012) showed that a high CCN concentration results in a high graupel/hail mass content through riming in their numerical modeling studies of deep convective clouds over Florida and the Southeast China, respectively. A recent numerical modeling study of aerosol loading effects on the amount of surface precipitation from deep convective clouds over the Indian peninsula during the monsoon season (Gayatri et al. 2017) also showed that the melting of graupel particles grown through active riming largely affects the surface precipitation amount in the high CCN case. On the other hand, this study shows that the increase in surface precipitation amount is mainly due to the melting of snow particles rather than graupel particles. One plausible reason for this difference in the results between the aforementioned studies and this study might have to do with the differences in the climates of the study regions. North central Mongolia is less humid than Florida, the Southeast China, and India. In a less humid region, the growths of graupel and hail particles seem to be not favorable since the drop mass content is smaller.

Figure 9 presents a schematic diagram that depicts microphysical processes and changes in hydrometeor mass contents that lead to the larger accumulated surface precipitation amount for higher aerosol number concentration in the aerosol number concentration range of $N_0 = 600$–4800 cm^{-3}. For a higher aerosol number concentration, more drops of small sizes form. More drops of small sizes grow through stronger condensation due to the larger total surface area of drops while being transported upward, and some of these transported drops freeze, which leads to an increase in the mass content of ice crystals. The increased ice crystal mass content leads to an increase in the mass content of small-sized snow particles largely through deposition. The increased mass content of small-sized snow particles leads to an increase in the mass content of large-sized snow particles largely through riming. Moreover, more drops of small sizes is responsible for an increase in the mass content of supercooled drops above the freezing level. The increased supercooled drop mass content leads to an increase in the mass content of large-sized snow particles through riming. More snow particles of large sizes, which result from these pathways, contribute to an increase in the amount of surface precipitation through melting and collision-coalescence.

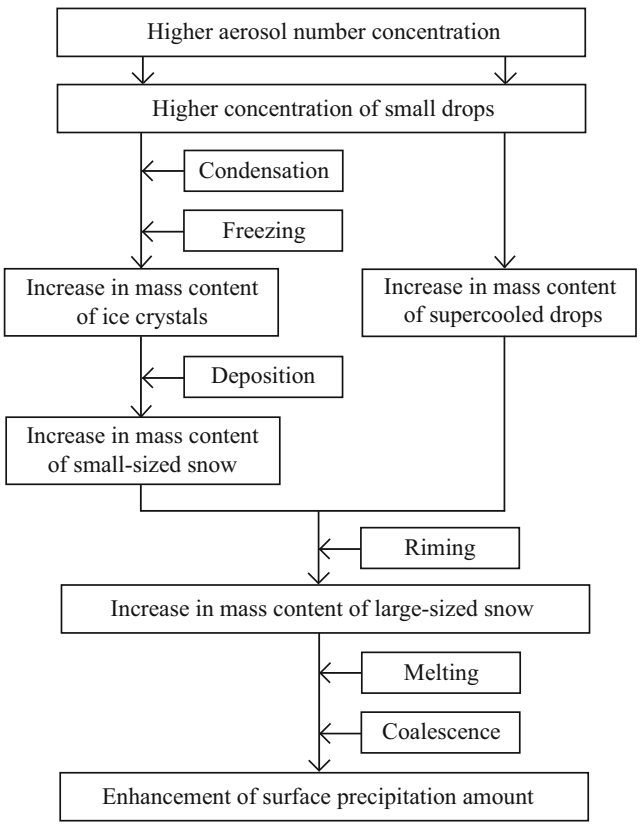

Fig. 9 Schematic diagram of main pathways of microphysical processes that lead to larger surface precipitation amount for higher aerosol number concentration

4 Summary and Conclusions

In this study, we investigated the impacts of changes in aerosol loading on surface precipitation from mid-latitude deep convective systems through simulations of a real case. For this, a precipitation event that occurred over north central Mongolia on 21 August 2014 was selected and simulations were performed with different initial aerosol number concentrations using the WRF model coupled with the updated bin microphysics scheme. The improved quasi-stochastic collection model which considers multiple collisions of cloud particles within a model time step is implemented in the bin microphysics scheme. It was found that the behavior of 24-h accumulated surface precipitation amount with aerosol number concentration is not monotonic. The 24-h accumulated surface precipitation amount slightly decreases with increasing aerosol number concentration in the range of $N_0 = 150$–600 cm^{-3}, while it notably increases with increasing aerosol number concentration in the range of $N_0 = 600$–4800 cm^{-3}. The 24-h accumulated surface precipitation amount in the case of $N_0 = 4800$ cm^{-3} is 22% larger than that in the case of $N_0 = 600$ cm^{-3}. Based upon the results of the analysis of mass contents and number concentrations of hydrometeors, mass change rates of hydrometeors and water vapor due to microphysical processes, and size distributions of hydrometeors, we have provided explanations as to why the accumulated surface precipitation amount increases with increasing aerosol number concentration in the range of $N_0 = 600$–4800 cm^{-3}. In brief, a higher aerosol number concentration leads to the increased mass content of large-sized snow particles which contributes to a larger surface precipitation amount through melting and collision-coalescence.

As shown in Fig. 4, the 24-h accumulated surface precipitation amount slightly decreases with increasing aerosol number concentration in the range of $N_0 = 150$–600 cm^{-3}. Changes in hydrometeor mass contents and relevant microphysical processes might be different from those depicted in Fig. 9. The impacts of aerosol loading on surface precipitation in the low aerosol concentration regime deserve an investigation. For this, additional simulations with much lower aerosol number concentrations are required.

In this study, we have attempted to explain reasons for the increase of accumulated surface precipitation amount with increasing aerosol number concentration in terms of changes in microphysics. It is well known that microphysics-dynamics interactions are important processes in deep convective clouds or systems. Hence, more extensive explanations would be possible if the microphysics-dynamics feedback is also analyzed, which is in need of a further investigation. Another interesting investigation would be to compare results simulated with bulk microphysics schemes and the bin microphysics scheme for examining aerosol loading impacts on surface precipitation. This kind of study can be helpful in improving parameterizations of cloud-aerosol interactions in bulk microphysics schemes.

In this study, horizontally uniform aerosol number concentration is used as an initial condition. Also, the aerosol module of the model, which solves the prognostic equation of aerosol number concentration in each bin, is simplified. The aerosol module includes nucleation scavenging and aerosol replenishment, but not dry scavenging and impaction scavenging. The present aerosol module needs to be further developed. Considering realistic spatio-temporal distribution of aerosols based on observations and more detailed aerosol-related processes not only improves the performance of precipitation prediction but also helps to better understand aerosol-cloud-precipitation interactions.

To further enhance our understanding of aerosol impacts on precipitation, more studies of real-case simulations in various geographical regions as well as well-designed idealized simulations using advanced numerical models need to be carried out. The present study is such an attempt. It reports the impacts of changes in aerosol loading on surface precipitation amount over north central Mongolia which is a high-altitude inland region.

Acknowledgements The authors are grateful to two anonymous reviewers for providing valuable comments on this study. The authors were supported by the Korea Meteorological Administration Research and Development Program under grants KMIPA 2015-5100. The authors thank supercomputer management division of the Korea Meteorological Administration for providing us with the supercomputer resource.

References

Alizadeh-Choobari, O., Gharaylou, M.: Aerosol impacts on radiative and microphysical properties of clouds and precipitation formation. Atmos. Res. **185**, 53–64 (2017)

Chen, F., Dudhia, J.: Coupling an advanced land surface–hydrology model with the Penn State–NCAR MM5 modeling system. Part I: model implementation and sensitivity. Mon. Weather Rev. **129**, 569–585 (2001)

Cheng, C.T., Wang, W.C., Chen, J.P.: A modelling study of aerosol impacts on cloud microphysics and radiative properties. Quart. J. Roy. Meteor. Soc. **133**, 283–297 (2007)

Choi, I.-J., Iguchi, T., Kim, S.-W., Nakajima, T., Yoon, S.-C.: The effect of aerosol representation on cloud microphysical properties in Northeast Asia. Meteor. Atmos. Phys. **123**, 181–194 (2014)

Clavner, M., Cotton, W. R., van den Heever, S.C., Saleeby, S.M., Pierce, J.R.: The response of a simulated mesoscale convective system to increased aerosol pollution: Part I: precipitation intensity, distribution, and efficiency. Atmos. Res. 199, 193–208 (2017)

Dagan, G., Koren, I., Altaratz, O., Heiblum, R.H.: Time-dependent, non-monotonic response of warm convective cloud fields to changes in aerosol loading. Atmos. Chem. Phys. **17**, 7435–7444 (2017)

Dee, D.P., Coauthors: The ERA-Interim reanalysis: configuration and performance of the data assimilation system. Quart. J. Roy. Meteor. Soc. **137**, 553–597 (2011)

Fan, J.W., Leung, L.R., Li, Z.Q., Morrison, H., Chen, H.B., Zhou, Y.Q., Qian, Y., Wang, Y.: Aerosol impacts on clouds and precipitation in

eastern China: results from bin and bulk microphysics. J. Geophys. Res. **117**, D00K36 (2012)

Fan, J.W., Wang, Y., Rosenfeld, D., Liu, X.: Review of aerosol-cloud interactions: mechanisms, significance, and challenges. J. Atmos. Sci. **73**, 4221–4252 (2016)

Gayatri, K., Patade, S., Prabhakaran, T.: Aerosol-cloud interaction in deep convective clouds over the Indian peninsula using spectral (bin) microphysics. J. Atmos. Sci. **74**, 3145–3166 (2017)

Han, J.-Y., Baik, J.-J., Khain, A.P.: A numerical study of urban aerosol impacts on clouds and precipitation. J. Atmos. Sci. **69**, 504–520 (2012)

Hong, S.-Y., Noh, Y., Dudhia, J.: A new vertical diffusion package with an explicit treatment of entrainment processes. Mon. Weather Rev. **134**, 2318–2341 (2006)

Houze, R. A., Jr.: Cloud dynamics, 2nd ed. Academic Press, pp 432. (2014)

Iacono, M.J., Delamere, J.S., Mlawer, E.J., Shephard, M.W., Clough, S.A., Collins, W.D.: Radiative forcing by long-lived greenhouse gases: calculations with the AER radiative transfer models. J. Geophys. Res. **113**, D13103 (2008)

Igel, A.L., van den Heever, S.C., Naud, C.M., Saleeby, S.M., Posselt, D.J.: Sensitivity of warm-frontal processes to cloud-nucleating aerosol concentrations. J. Atmos. Sci. **70**, 1768–1783 (2013)

Iguchi, T., Nakajima, T., Khain, A.P., Saito, K., Takemura, T., Okamoto, H., Nishizawa, T., Tao, W.-K.: Evaluation of cloud microphysics in JMA-NHM simulations using bin or bulk microphysical schemes through comparison with cloud radar observations. J. Atmos. Sci. **69**, 2566–2586 (2012)

Ilotoviz, E., Khain, A.P., Benmoshe, N., Phillips, V.T., Ryzhkov, A.V.: Effect of aerosols on freezing drops, hail, and precipitation in a midlatitude storm. J. Atmos. Sci. **73**, 109–144 (2016)

Jiang, Q., Wang, S.: Aerosol replenishment and cloud morphology: a VOCALS example. J. Atmos. Sci. **71**, 300–311 (2014)

Kain, J.S.: The Kain-Fritsch convective parameterization: an update. J. Appl. Meteorol. **43**, 170–181 (2004)

Khain, A.: Notes on state-of-the-art investigations of aerosol effects on precipitation: a critical review. Environ. Res. Lett. **4**, 015004 (2009)

Khain, A., Coauthors: Representation of microphysical processes in cloud-resolving models: spectral (bin) microphysics versus bulk parameterization. Rev. Geophys. **53**, 247–322 (2015)

Khain, A., Pokrovsky, A., Sednev, I.: Some effects of cloud aerosol interaction on cloud microphysics structure and precipitation formation: numerical experiments with a spectral microphysics cloud ensemble model. Atmos. Res. **52**, 195–220 (1999)

Khain, A., Ovtchinnikov, M., Pinsky, M., Pokrovsky, A., Krugliak, H.: Notes on the state-of-the-art numerical modeling of cloud microphysics. Atmos. Res. **55**, 159–224 (2000)

Khain, A., Rosenfeld, D., Pokrovsky, A.: Aerosol impact on the dynamics and microphysics of deep convective clouds. Quart. J. Roy. Meteor. Soc. **131**, 2639–2663 (2005)

Khain, A., Rosenfeld, D., Pokrovsky, A., Blahak, U., Ryzhkov, A.: The role of CCN in precipitation and hail in a mid-latitude storm as seen in simulations using a spectral (bin) microphysics model in a 2D dynamic frame. Atmos. Res. **99**, 129–146 (2011)

Kuba, N., Fujiyoshi, Y.: Development of a cloud microphysical model and parameterizations to describe the effect of CCN on warm cloud. Atmos. Chem. Phys. **6**, 2793–2810 (2006)

Lee, H., Baik, J.-J.: Effects of turbulence-induced collision enhancement on heavy precipitation: the 21 September 2010 case over the Korean peninsula. J. Geophys. Res. **121**, 12319–12342 (2016)

Lee, H., Baik, J.-J., Han, J.-Y.: Effects of turbulence on mixed-phase deep convective clouds under different basic-state winds and aerosol concentrations. J. Geophys. Res. **119**, 13506–13525 (2014)

Lee, S.S., Donner, L.J., Phillips, V.T., Ming, Y.: The dependence of aerosol effects on clouds and precipitation on cloud-system organization, shear and stability. J. Geophys. Res. **113**, D16202 (2008)

Li, G., Wang, Y., Zhang, R.: Implementation of a two-moment bulk microphysics scheme to the WRF model to investigate aerosol-cloud interaction. J. Geophys. Res. **113**, D15211 (2008)

Lkhamjav, J., Lee, H., Jeon, Y.-L., Baik, J.-J.: Examination of an improved quasi-stochastic model for the collisional growth of drops. J. Geophys. Res. **122**, 1713–1724 (2017a)

Lkhamjav, J., Jeon, Y.-L., Lee, H., Baik, J.-J., Seo, J.M.: Evaluation of the improved quasi-stochastic collection model through precipitation prediction over north central Mongolia. J. Geophys. Res. **122**, 13, 404–13,419 (2017b)

Lynn, B.H., Khain, A., Dudhia, J., Rosenfeld, D., Pokrovsky, A., Seifert, A.: Spectral (bin) microphysics coupled with a mesoscale model (MM5). Part I: model description and first results. Mon. Weather Rev. **133**, 44–58 (2005)

O'Halloran, T.L., Fuentes, J.D., Tao, W.K., Li, X.: Sensitivity of convection to observed variation in aerosol size distributions and composition at a rural site in the southeastern United States. J. Atmos. Chem. **72**, 441–454 (2015)

Rosenfeld, D., Lohmann, U., Raga, G.B., O'Dowd, C.D., Kulmala, M., Fuzzi, S., Reissell, A., Andreae, M.O.: Flood or drought: how do aerosols affect precipitation? Science. **321**, 1309–1313 (2008)

Sarangi, C., Tripathi, S.N., Kanawade, V.P., Koren, I., Pai, D.S.: Investigation of the aerosol-cloud-rainfall association over the Indian summer monsoon region. Atmos. Chem. Phys. **17**, 5185–5204 (2017)

Tao, W.-K., Li, X.: The relationship between latent heating, vertical velocity, and precipitation processes: the impact of aerosols on precipitation in organized deep convective systems. J. Geophys. Res. **121**, 6299–6320 (2016)

Tao, W.-K., Li, X., Khain, A., Matsui, T., Lang, S., Simpson, J.: Role of atmospheric aerosol concentration on deep convective precipitation: cloud-resolving model simulations. J. Geophys. Res. **112**, D24S18 (2007)

Tao, W.-K., Chen, J.-P., Li, Z., Wang, C., Zhang, C.: Impact of aerosols on convective clouds and precipitation. Rev. Geophys. **50**, RG2001 (2012)

Twomey, S.: Influence of pollution on shortwave albedo of clouds. J. Atmos. Sci. **34**, 1149–1152 (1977)

van den Heever, S.C., Carrio, G.G., Cotton, W.R., DeMott, P.J., Prenni, A.J.: Impacts of nucleating aerosol on Florida storms. Part I: mesoscale simulations. J. Atmos. Sci. **63**, 1752–1775 (2006)

Wang, C.: A modeling study of the response of tropical deep convection to the increase of cloud condensation nuclei concentration: 1. dynamics and microphysics. J. Geophys. Res. **110**, D21211 (2005)

Xiao, H., Yin, Y., Jin, L., Chen, Q., Chen, J.: Simulation of the effects of aerosol on mixed-phase orographic clouds using the WRF model with detailed bin microphysics scheme. J. Geophys. Res. **120**, 8345–8358 (2015)

Xue, H., Feingold, G.: Large-eddy simulations of trade wind cumuli: investigation of aerosol indirect effects. J. Atmos. Sci. **63**, 1605–1622 (2006)

Xue, L., Teller, A., Rasmussen, R., Geresdi, I., Pan, Z., Liu, X.: Effects of aerosol solubility and regeneration on mixed-phase orographic clouds and precipitation. J. Atmos. Sci. **69**, 1994–2010 (2012)

Zhou, X., Bei, N., Liu, H., Cao, J., Xing, L., Lei, W., Molina, L.T., Li, G.: Aerosol effects on the development of cumulus clouds over the Tibetan Plateau. Atmos. Chem. Phys. **17**, 7423–7434 (2017)